Extraordinary behaviors in a two-dimensional decoherent alternative quantum walk

Tian Chen* and Xiangdong Zhang
School of Physics, Beijing Institute of Technology, Beijing 100081, China
(Received 25 January 2016; published 11 July 2016)

We reveal the quantum and classical behaviors of the two-dimensional (2D) alternative quantum walk (AQW) in the presence of decoherence. For different kinds of decoherence, the analytic expressions for the moments of position distribution of the AQW are obtained. Taking the broken line noise and coin decoherence as examples of decoherence, we find that when decoherence emerges in only one direction, the anisotropic position distribution pattern appears, and not all the motions of the walker exhibit the transition from quantum to classical behaviors. Considering the effect of decoherence, we reveal the anisotropic correlations between the x (y) position of the 2D walker and the state of the coin in 2D AQWs.

DOI: 10.1103/PhysRevA.94.012316

I. INTRODUCTION

The quantum walk (QW) has been widely employed as a useful tool to design quantum algorithms, quantum gates, and quantum computation [1–18]. Due to the necessity of searching in a large database, multidimensional quantum fast search algorithms based on QWs have drawn lots of attention[10–15]. In the two-dimensional (2D) discrete-time quantum walk (DTQW), by introducing a four-level Grover coin into the evolution, the quantum Grover search algorithm has been realized in 2D position space [12,13]. The quantum search in a higher-dimensional hypercube has also been discussed [10,12,14,15]. When considering real experimental implementation, the physical system will have an inevitable interaction with the surrounding environment. Many studies of the DTQW report that due to the decoherence induced by the environment, the position distribution pattern of the QW changes to a binomial distribution that is similar to the distribution of a classical walk [19–35]. For the coherent QW, the variance of the position distribution in the QW increases quadratically with time, while with the introduction of decoherence into the walk, the variance of the position will increase linearly with time, which is a characteristic of the classical walk. In some sense, the emergence of decoherence in the QW converts the original QW into a classical walk.

Recently, a 2D QW with one two-level coin was presented [36–40]. In this alternative quantum walk (AQW), the two-level coin affects first the walker moving in the x direction, followed by the motion of the walker along the y direction. The position distribution pattern induced by the 2D DTQW with a four-level Grover coin can be recovered with the AQW with only one two-level coin [36,37]. Due to the function of the coin as the register of the coherence and randomness in the aforementioned DTQW, when the searching space increases to n dimensions, we need a 2^n-level coin to implement the search process. So in experiments, it is very difficult to realize a quantum Grover search in high dimensions with such a 2^n-level coin. Thanks to the reduction in resources of the AQW, this n-dimensional AQW is more feasible than the original DTQW with the 2^n-level coin [38]. The 2D AQW with one two-level coin has already been realized in experiments [41,42]. Because of the unavoidable interaction between the AQW and its surrounding environment, the decoherent effect of the environment on the dynamics of the AQW needs to be counted in a real-life QW experiment. Decoherence, including random phases, bit-flip noise, and phase-flip noise in the coin space, has been discussed for the 2D AQW [43–45]. The numerical results have revealed that classical behaviors emerge in the 2D AQW with increasing strength of the decoherence.

In this paper, we study the quantum and classical behaviors of the 2D AQW when the coin and the 2D walker undergo different kinds of decoherence. By employing the method presented in Refs. [20] and [30], we provide the analytic expressions for the first and second moments of position in the presence of any kind of decoherence. First, we take the broken-line-noise model as an example of the coin-position decoherence of the AQW, then we consider a 2D AQW involving coin decoherence where the coin is measured with a certain probability before each step of the walk. In our discussion, we assume that the decoherence emerges in the motion along the x direction of the 2D AQW. We study the position distribution of the 2D AQW and the variance of the position distribution with a change in the strength of the decoherence. In our work, we find that, for different kinds of decoherence, different quantum and classical behaviors emerge in the 2D AQW, and not motions along the x and the y direction of the AQW both exhibit a transition from quantum to classical behaviors. Different position distributions have been found between the 2D decoherent AQW and the four-level coin Grover walk [26]. What is more, we study the classical and quantum correlations between the x and the y positions of the 2D walker involving the coin-position decoherence or coin decoherence. Anisotropic patterns for the correlations between the x (y) position of the walker and the state of the coin have been found.

The organization of our work is as follows: the scheme of the 2D AQW incorporating the decoherence is introduced in Sec. II. The first and second moments of the position are addressed in analytic forms. Then in Sec. III, we take the broken-line-noise model and coin decoherence model as examples. The anisotropic behaviors for the variances in position and the anisotropic position distributions of the 2D AQW are presented. The correlations between the x (y) position of the walker and the coin in a 2D decoherent AQW are discussed in Sec. IV. The conclusion is given in Sec. V.

*chentian@bit.edu.cn

 ©2016 American Physical Society

II. MODEL

In the 2D AQW, there exists one 2D walker (the walker moves along the x and y directions) and one two-level coin ($|R\rangle$ and $|L\rangle$). The total Hilbert space for the 2D walker and coin is $\mathcal{H}_t = \mathcal{H}_x \otimes \mathcal{H}_y \otimes \mathcal{H}_c$. Here, $\mathcal{H}_x$ ($\mathcal{H}_y$) is an infinite-dimensional Hilbert space, and $\mathcal{H}_c$ is a two-level Hilbert space. The basis states of the space $\mathcal{H}_t$ are represented as $\{|x,y,c\rangle\}$, where x and y denote the position of the 2D walker along the x direction and y direction, respectively. The one-step evolution of the 2D AQW consists of two conditional shift operators and two coin operators, $U_w = S_y(I \otimes C)S_x(I \otimes C)$. The coin operator C is the Hadamard matrix, that is,

$$C = H = \frac{1}{\sqrt{2}}\begin{pmatrix} 1 & 1 \\ 1 & -1 \end{pmatrix}, \tag{1}$$

followed by the conditional shift operator along the x direction,

$$S_x = \sum_{i,j\in\mathbb{Z}} |i+1,j,R\rangle\langle i,j,R| + \sum_{i,j\in\mathbb{Z}} |i-1,j,L\rangle\langle i,j,L|. \tag{2}$$

After applying the operator C on the coin space, the conditional shift operator along the y direction is described as

$$S_y = \sum_{i,j\in\mathbb{Z}} |i,j+1,R\rangle\langle i,j,R| + \sum_{i,j\in\mathbb{Z}} |i,j-1,L\rangle\langle i,j,L|, \tag{3}$$

where $\mathbb{Z}$ denotes the x-y position space, which is spanned by the Hilbert space $\mathcal{H}_x$ and $\mathcal{H}_y$. It has been verified that when the walker starts from the position $|0\rangle_x|0\rangle_y$, with an appropriate choice of the initial coin state, the position distribution of the 2D AQW at time t is the same as that from the 2D DTQW with a four-level Grover coin [36,37].

Due to the inevitable interaction with the surrounding environment, the evolution of the coherent AQW is affected by noise. The one-step evolution of a system comprising a walker and a coin can be written in the form of the Kraus operators [46],

$$\rho(t+1) = \sum_{n=1}^{m} E_n \rho(t) E_n^\dagger. \tag{4}$$

Here, the term E_n is the Kraus operators containing the influence on the system from the environment. The general form of E_n is $E_n = \sum_{x,y}\sum_{l_1,l_2}\sum_{q,s} a^{(n)}_{x,l_1,y,l_2,q,s}|x+l_1\rangle\langle x| \otimes |y+l_2\rangle\langle y| \otimes |q\rangle\langle s|$, where $x,l_1,y,l_2 = -\infty,\ldots,+\infty$ and $q,s = \{L,R\}$. The function of the Kraus operators is associated with the coefficient $a^{(n)}_{x,l_1,y,l_2,q,s}$. In the discussion below, we assume that the coefficient $a^{(n)}_{x,l_1,y,l_2,q,s}$ does not depend on the coordinates x and y. This means that the probability of translation in the position space depends only on the distances l_1 and l_2 of the translation. So the coefficient $a^{(n)}_{x,l_1,y,l_2,q,s}$ changes to a simple form, $a^{(n)}_{l_1,l_2,q,s}$. The complete relation for the Kraus operators is $\sum_{n=1}^{m} E_n^\dagger E_n = \mathbb{I}$. The Kraus operators E_n can be expressed in a general form,

$$E_n = \langle e_n|U|\text{env}\rangle. \tag{5}$$

Here, the evolution operator U acts on the total system including the system and the environment. The one-step evolution for the system is expressed as

$$\rho(t+1) = \sum_{n=1}^{s} E_n \rho(t) E_n^\dagger = \sum_{n=1}^{s} f_n W_n \rho(t) W_n^\dagger, \tag{6}$$

where the coefficient f_n denotes the probability that the nth resource from the environment affects the system dynamics. In the discussion below, the role of the system is represented by the 2D walker and the coin of the 2D AQW, and the evolution of the system is affected by noise from the surrounding environment. The effect on the system is described by the operator W_n, and the relation between the Kraus operator E_n and the operator W_n is

$$E_n = \sqrt{f_n} W_n. \tag{7}$$

Considering that the evolution for the total system (system + environment) is unitary, the total evolution operator U for the total system can be addressed as [20,30]

$$U = |e_1\rangle\langle e_1| \otimes W_1 + \cdots + |e_s\rangle\langle e_s| \otimes W_s, \tag{8}$$

where, for the environment state $|e_n\rangle$, the effect on the system is described by the corresponding operator W_n. Understanding the exact form of the environment is not required, and the effects of the environment on the system are contained in different operators W_n. With the introduction of the initial state for the environment as

$$|\text{env}\rangle = \sqrt{f_1}|e_1\rangle + \sqrt{f_2}|e_2\rangle + \cdots + \sqrt{f_s}|e_s\rangle, \tag{9}$$

the form of the Kraus operator E_n is obtained [Eq. (5)] and the system evolution can be described with Eq. (6).

To illustrate the system dynamics, we apply the Fourier transform to analyze the dynamics of the 2D AQW [20,30]. The transformations along the x and y directions can be addressed as

$$\begin{aligned} |x\rangle &= \int_{-\pi}^{\pi} \frac{dk}{2\pi} e^{-ikx}|k\rangle, \\ |y\rangle &= \int_{-\pi}^{\pi} \frac{dp}{2\pi} e^{-ipy}|p\rangle. \end{aligned} \tag{10}$$

Based on the equations above, we can formulate the expression for the element of position distribution as

$$\begin{aligned} &\sum_{x,y} |x+l_1,y+l_2\rangle\langle x,y| \\ &= \frac{1}{(2\pi)^2}\int_{-\pi}^{\pi}\int_{-\pi}^{\pi} dkdp e^{-il_1k-il_2p}|k,p\rangle\langle k,p|. \end{aligned} \tag{11}$$

The Kraus operator E_n can be obtained in the form

$$E_n = \frac{1}{(2\pi)^2}\int_{-\pi}^{\pi}\int_{-\pi}^{\pi} dkdp|k\rangle\langle k| \otimes |p\rangle\langle p| \otimes F_n(k,p). \tag{12}$$

The operator $F_n(k,p)$ takes the form $F_n(k,p) = \sum_{l_1,l_2}\sum_{q,s} a^{(n)}_{l_1,l_2,q,s} e^{-il_1k}e^{-il_2p}|q\rangle\langle s|$, which acts on the coin space. With the assumption that the 2D walker starts from the position (0,0) in the x-y plane, the initial density matrix for the system is

$$\rho_0 = \iiint\!\!\int \frac{dkdk'}{4\pi^2}\frac{dpdp'}{4\pi^2}|k\rangle\langle k'| \otimes |p\rangle\langle p'| \otimes |\psi_0\rangle\langle\psi_0|, \tag{13}$$

where the initial state of the coin is represented by $|\psi_0\rangle$. After one step of evolution, the system can be formulated as

$$\rho' = \sum_{n=1}^{m} E_n \rho_0 E_n^\dagger = \iiiint \frac{dkdk'}{4\pi^2}\frac{dpdp'}{4\pi^2}|k\rangle\langle k'| \otimes |p\rangle\langle p'| \otimes \mathcal{L}_{k,k',p,p'}|\psi_0\rangle\langle\psi_0|, \tag{14}$$

with $\mathcal{L}_{k,k',p,p'}\tilde{O} = \sum_n F_n(k,p)\tilde{O}F_n^\dagger(k',p')$. Thus, the system density matrix after t step evolution can be obtained as

$$\rho(t) = \iiiint \frac{dkdk'}{4\pi^2}\frac{dpdp'}{4\pi^2}|k\rangle\langle k'| \otimes |p\rangle\langle p'| \otimes \mathcal{L}^t_{k,k',p,p'}|\psi_0\rangle\langle\psi_0|. \tag{15}$$

So at time t, the probability of the 2D walker's occupying position (x,y) is

$$P(x,y,t) = \mathrm{Tr}_{x,y,c}[\rho(t)] = \frac{1}{(2\pi)^4}\iiiint dkdk'dpdp'e^{-ix(k'-k)}e^{-iy(p'-p)}\mathrm{Tr}\big(\mathcal{L}^t_{k,k',p,p'}|\psi_0\rangle\langle\psi_0|\big). \tag{16}$$

The mth moments of the probability distribution $\langle x^m\rangle$ and $\langle y^m\rangle$ for the 2D AQW are defined as

$$\langle x^m\rangle = \sum_{x,y} x^m P(x,y,t) = \frac{1}{(2\pi)^3}\sum_x x^m \iiint dkdk'dpe^{-ix(k'-k)}\mathrm{Tr}\big(\mathcal{L}^t_{k,k',p,p'}|\psi_0\rangle\langle\psi_0|\big),$$

$$\langle y^m\rangle = \sum_{x,y} y^m P(x,y,t) = \frac{1}{(2\pi)^3}\sum_y y^m \iiint dkdk'dpe^{-iy(p'-p)}\mathrm{Tr}\big(\mathcal{L}^t_{k,k',p,p'}|\psi_0\rangle\langle\psi_0|\big). \tag{17}$$

Based on the expressions for the mth moments of the position distribution, we can obtain the analytic forms for the first and second moments $\langle x\rangle$, $\langle y\rangle$, $\langle x^2\rangle$, and $\langle y^2\rangle$ in the presence of decoherence as

$$\langle x\rangle = \frac{i}{(2\pi)^2}\iint dkdp\sum_{m=1}^{t}\mathrm{Tr}\big(\mathcal{K}_{k,p}\mathcal{L}^{m-1}_{k,p}|\psi_0\rangle\langle\psi_0|\big), \quad \langle y\rangle = \frac{i}{(2\pi)^2}\iint dkdp\sum_{n=1}^{t}\mathrm{Tr}\big(\mathcal{P}_{k,p}\mathcal{L}^{n-1}_{k,p}|\psi_0\rangle\langle\psi_0|\big),$$

$$\langle x^2\rangle = \frac{1}{(2\pi)^2}\iint dkdp\sum_{m=1}^{t}\sum_{m'=1}^{m-1}\big\{\mathrm{Tr}\big[\mathcal{K}_{k,p}\mathcal{L}^{m-m'-1}_{k,p}\big(\mathcal{K}^\dagger_{k,p}\mathcal{L}^{m'-1}_{k,p}|\psi_0\rangle\langle\psi_0|\big)\big]$$

$$+\mathrm{Tr}\big[\mathcal{K}^\dagger_{k,p}\mathcal{L}^{m-m'-1}_{k,p}\big(\mathcal{K}_{k,p}\mathcal{L}^{m'-1}_{k,p}|\psi_0\rangle\langle\psi_0|\big)\big]\big\} + \frac{1}{(2\pi)^2}\iint dkdp\sum_{m=1}^{t}\mathrm{Tr}[\mathcal{T}_k(\mathcal{L}^{m-1}_{k,p}|\psi_0\rangle\langle\psi_0|)],$$

$$\langle y^2\rangle = \frac{1}{(2\pi)^2}\iint dkdp\sum_{n=1}^{t}\sum_{n'=1}^{n-1}\big\{\mathrm{Tr}\big[\mathcal{P}_{k,p}\mathcal{L}^{n-n'-1}_{k,p}\big(\mathcal{P}^\dagger_{k,p}\mathcal{L}^{n'-1}_{k,p}|\psi_0\rangle\langle\psi_0|\big)\big]$$

$$+\mathrm{Tr}\big[\mathcal{P}^\dagger_{k,p}\mathcal{L}^{n-n'-1}_{k,p}\big(\mathcal{P}_{k,p}\mathcal{L}^{n'-1}_{k,p}|\psi_0\rangle\langle\psi_0|\big)\big]\big\} + \frac{1}{(2\pi)^2}\iint dkdp\sum_{n=1}^{t}\mathrm{Tr}\big[\mathcal{T}_p\big(\mathcal{L}^{n-1}_{k,p}|\psi_0\rangle\langle\psi_0|\big)\big]. \tag{18}$$

Here, the superoperators $\mathcal{K}_{k,p}$, $\mathcal{K}^\dagger_{k,p}$, $\mathcal{T}_k$, $\mathcal{P}_{k,p}$, $\mathcal{P}^\dagger_{k,p}$, and $\mathcal{T}_p$ above are represented by the explicit expressions as $\mathcal{K}_{k,p}\tilde{O} = \sum_n \frac{\partial F_n}{\partial k}\tilde{O}F_n^\dagger$, $\mathcal{K}^\dagger_{k,p}\tilde{O} = \sum_n F_n\tilde{O}\frac{\partial F_n^\dagger}{\partial k}$, $\mathcal{T}_k\tilde{O} = \sum_n \frac{\partial F_n}{\partial k}\tilde{O}\frac{\partial F_n^\dagger}{\partial k}$, $\mathcal{P}_{k,p}\tilde{O} = \sum_n \frac{\partial F_n}{\partial p}\tilde{O}F_n^\dagger$, $\mathcal{P}^\dagger_{k,p}\tilde{O} = \sum_n F_n\tilde{O}\frac{\partial F_n^\dagger}{\partial p}$, and $\mathcal{T}_p\tilde{O} = \sum_n \frac{\partial F_n}{\partial p}\tilde{O}\frac{\partial F_n^\dagger}{\partial p}$.

Based on the equations above, we have obtained the expressions for the moments of the position distribution [Eqs. (17) and (18)] for a 2D AQW in the presence of different kinds of decoherence. In the following, we take the broken line noise and coin decoherence as explicit forms of decoherence and study the behaviors of a 2D AQW under these two kinds of decoherence.

III. TWO KINDS OF DECOHERENCE FOR THE TWO-DIMENSIONAL AQW

In this section, first, we take the broken-line-noise model as an example of coin-position decoherence, then the coin decoherence is introduced into a walk in which the coin is measured with a certain probability before each step of the walk. We study the variances of the position distribution and diffusion coefficients of these 2D decoherent AQWs. The anisotropic position distribution patterns of these two decoherent AQWs are presented later.

A. The broken-line-noise model

In the QW, the walker moves from one position to adjacent positions controlled by the current state of the coin. Compared with the classical walk, the interference between wave functions at different positions leads to different behaviors in the QW. For the QW, the broken-line-noise model denotes one kind of decoherence where the connection between the position and the adjacent positions is broken with a certain probability [22,26,30]. Here, we assume that the broken line noise appears only in the x direction, and four possible evolutions of the 2D AQW involving decoherence are depicted in Fig. 1.

In Fig. 1, first, the walker moves in the x direction, labeled by the green arrows along the horizontal direction;

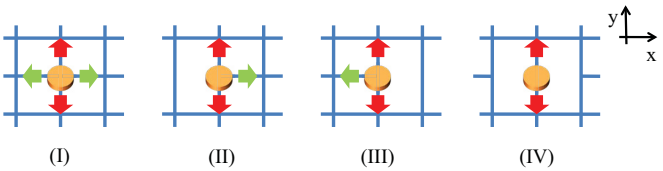

FIG. 1. Schematic of a 2D AQW with broken line noise; the noise is applied only along the x direction. Four possible cases of an AQW are shown: (I) there is no decoherence, with probability $(1-f)^2$; (II) the connection between the position and its left adjacent position is broken, with probability $f(1-f)$; (III) the connection between the position and its right adjacent position is broken, with probability $f(1-f)$; and (IV) the connections between the position and its adjacent positions (left and right) are broken, with probability f^2.

then the walker travels along the y direction, labeled by the red arrows along the vertical direction. The 2D AQW without decoherence is addressed in Fig. 1, (I), with probability $(1-f)^2$. The connection between the current position and the left adjacent position is broken with probability $f(1-f)$, which is addressed in Fig. 1, (II). In Fig. 1, (III), the connection between the current position and the right adjacent position is cut off with probability $f(1-f)$. In Fig. 1, (IV), neither the right neighbor nor the left neighbor has any connection with the current position, and the motion along the x direction is trapped with probability f^2. To obtain these four possible evolutions with certain probabilities presented in Fig. 1, we can introduce the initial state of the environment as

$$|\mathrm{env}\rangle = (1-f)|e_1\rangle + \sqrt{f(1-f)}|e_2\rangle + \sqrt{f(1-f)}|e_3\rangle + f|e_4\rangle. \tag{19}$$

When the state of the environment is $|e_n\rangle$ $(n = 1,2,3,4)$, the corresponding Kraus operator E_n $(n = 1,2,3,4)$ is applied to the system [see Eq. (5)]. The explicit expressions of E_n $(n = 1,2,3,4)$ are

$$\begin{aligned}
E_1 &= (1-f)\sum_{x,y}\frac{1}{2}\{|x+1,y+1\rangle\langle x,y|\otimes(|R\rangle\langle R| + |R\rangle\langle L|) + |x+1,y-1\rangle\langle x,y|\otimes(|L\rangle\langle R| + |L\rangle\langle L|) \\
&\quad + |x-1,y+1\rangle\langle x,y|(-|R\rangle\langle L| + |R\rangle\langle R|) + |x-1,y-1\rangle\langle x,y|(-|L\rangle\langle R| + |L\rangle\langle L|)\}, \qquad (20a)\\
E_2 &= \sqrt{f(1-f)}\sum_{x,y}\frac{1}{2}\{|x+1,y+1\rangle\langle x,y|\otimes(|R\rangle\langle R| + |R\rangle\langle L|) + |x+1,y-1\rangle\langle x,y|\otimes(|L\rangle\langle R| + |L\rangle\langle L|) \\
&\quad + |x,y+1\rangle\langle x,y|(-|R\rangle\langle L| + |R\rangle\langle R|) + |x,y-1\rangle\langle x,y|(|L\rangle\langle R| - |L\rangle\langle L|)\}, \qquad (20b)\\
E_3 &= \sqrt{f(1-f)}\sum_{x,y}\frac{1}{2}\{|x,y+1\rangle\langle x,y|\otimes(|R\rangle\langle R| + |R\rangle\langle L|) + |x,y-1\rangle\langle x,y|\otimes(-|L\rangle\langle R| - |L\rangle\langle L|) \\
&\quad + |x-1,y+1\rangle\langle x,y|(|R\rangle\langle L| - |R\rangle\langle R|) + |x-1,y-1\rangle\langle x,y|(|L\rangle\langle R| - |L\rangle\langle L|)\}, \qquad (20c)\\
E_4 &= f\sum_{x,y}\{|x,y+1\rangle\langle x,y|\otimes|R\rangle\langle R| - |x,y-1\rangle\langle x,y|\otimes|L\rangle\langle L|\}. \qquad (20d)
\end{aligned}$$

For each Kraus operator E_n $(n = 1, 2, 3, 4)$, we obtain the corresponding operator in the coin space F_n $(n = 1, 2, 3, 4)$ as

$$\begin{aligned}
F_1 &= (1-f)\begin{pmatrix} \frac{1}{2}e^{-i(k+p)} + \frac{1}{2}e^{i(k-p)} & \frac{1}{2}e^{-i(k+p)} - \frac{1}{2}e^{i(k-p)} \\ \frac{1}{2}e^{-i(k-p)} - \frac{1}{2}e^{i(k+p)} & \frac{1}{2}e^{-i(k-p)} + \frac{1}{2}e^{i(k+p)} \end{pmatrix}, \qquad (21a)\\
F_2 &= \sqrt{f(1-f)}\begin{pmatrix} \frac{1}{2}e^{-i(k+p)} + \frac{1}{2}e^{-ip)} & \frac{1}{2}e^{-i(k+p)} - \frac{1}{2}e^{-ip} \\ \frac{1}{2}e^{-i(k-p)} + \frac{1}{2}e^{ip} & \frac{1}{2}e^{-i(k-p)} - \frac{1}{2}e^{ip} \end{pmatrix}, \qquad (21b)\\
F_3 &= \sqrt{(1-f)}\begin{pmatrix} \frac{1}{2}e^{-ip} - \frac{1}{2}e^{i(k-p)} & \frac{1}{2}e^{-ip} + \frac{1}{2}e^{i(k-p)} \\ -\frac{1}{2}e^{ip} + \frac{1}{2}e^{i(k+p)} & -\frac{1}{2}e^{ip} - \frac{1}{2}e^{i(k+p)} \end{pmatrix}, \qquad (21c)\\
F_4 &= f\begin{pmatrix} e^{-ip} & 0 \\ 0 & -e^{ip} \end{pmatrix}. \qquad (21d)
\end{aligned}$$

The complete relation is satisfied with $\sum_n F_n^\dagger F_n = I$. To calculate the moments of the position ($\langle x\rangle$, $\langle y\rangle$, $\langle x^2\rangle$, and $\langle y^2\rangle$), we employ one representation that transforms one 2×2 matrix to one 4×1 column vector [20,30]; that is,

$$\tilde{O} = r_0 I + r_1\sigma_x + r_2\sigma_y + r_3\sigma_z = \begin{pmatrix} r_0 \\ r_1 \\ r_2 \\ r_3 \end{pmatrix}. \tag{22}$$

Using this representation, the superoperators $\mathcal{L}_{k,p}$, $\mathcal{K}_{k,p}$, $\mathcal{T}_k$, $\mathcal{P}_{k,p}$, and $\mathcal{T}_p$ of the 2D AQW involving broken line noise can be obtained in matrix form as

$$\mathcal{L}_{k,p}\tilde{O} = \begin{pmatrix} 1 & 0 & 0 & 0 \\ 0 & (1-2f)\cos 2p & 2f(1-f)\sin k\cos 2p - (1-f)^2\cos 2k\sin 2p + f^2\sin 2p & (1-f)^2\sin 2k\sin 2p + 2f(1-f)\cos k\cos 2p \\ 0 & (1-2f)\sin 2p & (1-f)^2\cos 2k\cos 2p + 2f(1-f)\sin k\sin 2p - f^2\cos 2p & 2f(1-f)\cos k\sin 2p - (1-f)^2\cos 2p\sin 2k \\ 0 & 0 & (1-f)^2\sin 2k & (1-f)^2\cos 2k + f^2 \end{pmatrix} \begin{pmatrix} r_0 \\ r_1 \\ r_2 \\ r_3 \end{pmatrix}, \tag{23}$$

$$\mathcal{K}_{k,p}\tilde{O} = \begin{pmatrix} 0 & -i(1-f) & -if(1-f)\sin k & -if(1-f)\cos k \\ -i(1-f)\cos 2p & 0 & f(1-f)\cos k\cos 2p + (1-f)^2\sin 2k\sin 2p & (1-f)^2\cos 2k\sin 2p - f(1-f)\sin k\cos 2p \\ -i(1-f)\sin 2p & 0 & f(1-f)\cos k\sin 2p - (1-f)^2\sin 2k\cos 2p & -f(1-f)\sin k\sin 2p - (1-f)^2\cos 2p\cos 2k \\ 0 & 0 & (1-f)^2\cos 2k & -(1-f)^2\sin 2k \end{pmatrix} \begin{pmatrix} r_0 \\ r_1 \\ r_2 \\ r_3 \end{pmatrix}, \tag{24}$$

$$\mathcal{T}_k\tilde{O} = \begin{pmatrix} 1-f & 0 & 0 & 0 \\ 0 & \cos 2p(1-f) & (1-f)^2\cos 2k\sin 2p & -(1-f)^2\sin 2k\sin 2p \\ 0 & \sin 2p(1-f) & -(1-f)^2\cos 2k\cos 2p & (1-f)^2\cos 2p\sin 2k \\ 0 & 0 & -(1-f)^2\sin 2k & -(1-f)^2\cos 2k \end{pmatrix} \begin{pmatrix} r_0 \\ r_1 \\ r_2 \\ r_3 \end{pmatrix}, \tag{25}$$

$$\mathcal{P}_{k,p}\tilde{O} = \begin{pmatrix} 0 & 0 & -i(1-f)^2\sin 2k & -i(1-f)^2\cos 2k - if^2 \\ 0 & (2f-1)\sin 2p & -(1-f)^2\cos 2k\cos 2p - 2f(1-f)\sin k\sin 2p + f^2\cos 2p & (1-f)^2\sin 2k\cos 2p - 2f(1-f)\cos k\sin 2p \\ 0 & (1-2f)\cos 2p & -(1-f)^2\cos 2k\sin 2p + 2f(1-f)\sin k\cos 2p + f^2\sin 2p & (1-f)^2\sin 2k\sin 2p + 2f(1-f)\cos k\cos 2p \\ -i & 0 & 0 & 0 \end{pmatrix} \begin{pmatrix} r_0 \\ r_1 \\ r_2 \\ r_3 \end{pmatrix}, \tag{26}$$

$$\mathcal{T}_p\tilde{O} = \begin{pmatrix} 1 & 0 & 0 & 0 \\ 0 & \cos 2p(2f-1) & (1-f)^2\cos 2k\sin 2p - 2f(1-f)\sin k\cos 2p - f^2\sin 2p & -(1-f)^2\sin 2k\sin 2p - 2f(1-f)\cos k\cos 2p \\ 0 & \sin 2p(2f-1) & -(1-f)^2\cos 2k\cos 2p - 2f(1-f)\sin k\sin 2p + f^2\cos 2p & (1-f)^2\cos 2p\sin 2k - 2f(1-f)\cos k\sin 2p \\ 0 & 0 & (1-f)^2\sin 2k & f^2 + (1-f)^2\cos 2k \end{pmatrix} \begin{pmatrix} r_0 \\ r_1 \\ r_2 \\ r_3 \end{pmatrix}, \tag{27}$$

where $\mathcal{K}_{k,p}^{\dagger}\tilde{O} = \mathcal{K}^*\tilde{O}$, $\mathcal{P}_{k,p}^{\dagger}\tilde{O} = \mathcal{P}^*\tilde{O}$, and the initial coin state $|\psi_0\rangle$ is set as

$$|\psi_0\rangle\langle\psi_0| = \begin{pmatrix} r_0 \\ r_1 \\ r_2 \\ r_3 \end{pmatrix}. \tag{28}$$

Considering the expression of the superoperator $\mathcal{L}$, we can verify that

$$\mathcal{L}_{k,p}^{m-1}|\psi_0\rangle\langle\psi_0| = \begin{pmatrix} r_0 \\ r_1' \\ r_2' \\ r_3' \end{pmatrix}. \tag{29}$$

The first-row element r_0 remains unchanged when any times of $\mathcal{L}$ are applied. When taking into account the trace operator, we obtain the results related to the operators $\mathcal{T}_k$ and $\mathcal{T}_p$:

$$\sum_{m=1}^{t}\mathrm{Tr}\big[\mathcal{T}_k\big(\mathcal{L}_{k,p}^{m-1}|\psi_0\rangle\langle\psi_0|\big)\big] = 2(1-f)t\cdot r_0, \quad \sum_{n=1}^{t}\mathrm{Tr}\big[\mathcal{T}_p\big(\mathcal{L}_{k,p}^{n-1}|\psi_0\rangle\langle\psi_0|\big)\big] = 2r_0 t. \tag{30}$$

Considering the expressions of the superoperators, the first-row element r_0 of the 4×1 column vector makes no contribution to the moments $\langle x^2\rangle$ and $\langle y^2\rangle$ [Eq. (18)], so we can omit the outcomes associated with r_0 and obtain the first term of the second moments $\langle x^2\rangle$, $\langle y^2\rangle$ as

$$\begin{aligned} &\sum_{m=1}^{t}\sum_{m'=1}^{m-1}\big\{\mathrm{Tr}\big[\mathcal{K}_{k,p}\mathcal{L}_{k,p}^{m-m'-1}\big(\mathcal{K}_{k,p}^{\dagger}\mathcal{L}_{k,p}^{m'-1}|\psi_0\rangle\langle\psi_0|\big)\big] + \mathrm{Tr}\big[\mathcal{K}_{k,p}^{\dagger}\mathcal{L}_{k,p}^{m-m'-1}\big(\mathcal{K}_{k,p}\mathcal{L}_{k,p}^{m'-1}|\psi_0\rangle\langle\psi_0|\big)\big]\big\} \\ &= 4(1-f, f(1-f)\sin k, f(1-f)\cos k)\sum_{m=1}^{t}\sum_{m'=1}^{m-1}\mathcal{M}_{k,p}^{m-m'-1}\begin{pmatrix}(1-f)\cos 2p\cdot r_0 \\ (1-f)\sin 2p\cdot r_0 \\ 0\end{pmatrix} \\ &= 2(1-f, f(1-f)\sin k, f(1-f)\cos k)(I-\mathcal{M}_{k,p})^{-1}\left\{t - \frac{\mathcal{M}_{k,p}}{I-\mathcal{M}_{k,p}}\right\}\begin{pmatrix}(1-f)\cos 2p \\ (1-f)\sin 2p \\ 0\end{pmatrix}, \end{aligned} \tag{31}$$

$$\sum_{n=1}^{t}\sum_{n'=1}^{n-1}\left\{\mathrm{Tr}\left[\mathcal{P}_{k,p}\mathcal{L}_{k,p}^{n-n'-1}\left(\mathcal{P}_{k,p}^{\dagger}\mathcal{L}_{k,p}^{m'-1}|\psi_0\rangle\langle\psi_0|\right)\right]+\mathrm{Tr}\left[\mathcal{P}_{k,p}^{\dagger}\mathcal{L}_{k,p}^{n-n'-1}\left(\mathcal{P}_{k,p}\mathcal{L}_{k,p}^{n'-1}|\psi_0\rangle\langle\psi_0|\right)\right]\right\}$$
$$=4(0,(1-f)^2\sin 2k,(1-f)^2\cos 2k+f^2)\sum_{n=1}^{t}\sum_{n'=1}^{n-1}\mathcal{M}_{k,p}^{n-n'-1}\begin{pmatrix}0\\0\\r_0\end{pmatrix}$$
$$=2(0,(1-f)^2\sin 2k,(1-f)^2\cos 2k+f^2)(I-\mathcal{M}_{k,p})^{-1}\left\{t-\frac{\mathcal{M}_{k,p}}{I-\mathcal{M}_{k,p}}\right\}\begin{pmatrix}0\\0\\1\end{pmatrix}, \tag{32}$$

where r_0 is chosen as $r_0 = 1/2$ for the normalization of the initial state $|\psi_0\rangle$. The term $\mathcal{M}_{k,p}$ is a 3×3 matrix,

$$\mathcal{M}_{k,p}\tilde{O}=\begin{pmatrix}(1-2f)\cos 2p & 2f(1-f)\sin k\cos 2p-(1-f)^2\cos 2k\sin 2p+f^2\sin 2p & (1-f)^2\sin 2k\sin 2p+2f(1-f)\cos k\cos 2p\\ (1-2f)\sin 2p & (1-f)^2\cos 2k\cos 2p+2f(1-f)\sin k\sin 2p-f^2\cos 2p & 2f(1-f)\cos k\sin 2p-(1-f)^2\cos 2p\sin 2k\\ 0 & (1-f)^2\sin 2k & (1-f)^2\cos 2k+f^2\end{pmatrix}\begin{pmatrix}r_1\\r_2\\r_3\end{pmatrix}. \tag{33}$$

Based on the equations addressed above, the first moments of positions $\langle x\rangle$ and $\langle y\rangle$ for the 2D AQW with broken line noise are presented as

$$\begin{aligned}\langle x\rangle &= \frac{i}{2\pi^2}\iint dkdp(-i)\begin{pmatrix}1-f\\ f(1-f)\sin k\\ f(1-f)\cos k\end{pmatrix}^{T}\left[\sum_{m=1}^{t}\mathcal{M}_{k,p}^{m-1}\right]\begin{pmatrix}r_1\\r_2\\r_3\end{pmatrix}\\ &= \frac{1}{2\pi^2}\iint dkdp\begin{pmatrix}1-f\\ f(1-f)\sin k\\ f(1-f)\cos k\end{pmatrix}^{T}(I-\mathcal{M}_{k,p})^{-1}\begin{pmatrix}r_1\\r_2\\r_3\end{pmatrix},\\ \langle y\rangle &= \frac{i}{2\pi^2}\iint dkdp(-i)\begin{pmatrix}0\\ (1-f)^2\sin 2k\\ (1-f)^2\cos 2k+f^2\end{pmatrix}^{T}\left[\sum_{n=1}^{t}\mathcal{M}_{k,p}^{n-1}\right]\begin{pmatrix}r_1\\r_2\\r_3\end{pmatrix}\\ &= \frac{1}{2\pi^2}\iint dkdp\begin{pmatrix}0\\ (1-f)^2\sin 2k\\ (1-f)^2\cos 2k+f^2\end{pmatrix}^{T}(I-\mathcal{M}_{k,p})^{-1}\begin{pmatrix}r_1\\r_2\\r_3\end{pmatrix},\end{aligned} \tag{34}$$

where the superscript T stands for the transpose on that matrix, and the second moments of positions $\langle x^2\rangle$ and $\langle y^2\rangle$ for the 2D AQW with broken line noise are addressed as

$$\begin{aligned}\langle x^2\rangle &= \frac{1}{2\pi^2}\iint dkdp\left\{\begin{pmatrix}1-f\\ f(1-f)\sin k\\ f(1-f)\cos k\end{pmatrix}^{T}(I-\mathcal{M}_{k,p})^{-1}\left[t-\frac{\mathcal{M}_{k,p}}{I-\mathcal{M}_{k,p}}\right]\cdot\begin{pmatrix}(1-f)\cos 2p\\ (1-f)\sin 2p\\ 0\end{pmatrix}\right\}+\frac{1}{2\pi^2}\iint dkdp\frac{1}{2}(1-f)t,\\ \langle y^2\rangle &= \frac{1}{2\pi^2}\iint dkdp\left\{\begin{pmatrix}0\\ (1-f)^2\sin 2k\\ (1-f)^2\cos 2k+f^2\end{pmatrix}^{T}(I-\mathcal{M}_{k,p})^{-1}\cdot\left[t-\frac{\mathcal{M}_{k,p}}{I-\mathcal{M}_{k,p}}\right]\begin{pmatrix}0\\0\\1\end{pmatrix}\right\}+\frac{1}{2\pi^2}\iint dkdp\frac{1}{2}t.\end{aligned} \tag{35}$$

To illustrate the transition from quantum to classical behaviors in the 2D AQW involving broken line noise, we calculate the diffusion coefficients D_x and D_y as

$$
\begin{aligned}
D_x =& \frac{1}{2}\lim_{t\to\infty}\frac{\partial\sigma_x^2}{\partial t} = \frac{1}{2}\lim_{t\to\infty}\frac{\partial(\langle x^2\rangle - \langle x\rangle^2)}{\partial t} \\
=& \frac{1}{2}\left\{\frac{1}{2\pi^2}\iint dkdp \begin{pmatrix} 1-f \\ f(1-f)\sin k \\ f(1-f)\cos k \end{pmatrix}^T (I-\mathcal{M}_{k,p})^{-1}\begin{pmatrix}(1-f)\cos 2p \\ (1-f)\sin 2p \\ 0\end{pmatrix} + (1-f)\right\} \\
=& \frac{1-f}{2f}\left[\frac{1}{2\pi^2}\iint dkdp\frac{(1-f)}{2}R_x(f,k,p) + f\right] = \frac{1-f}{2f}B_x(f), \\
D_y =& \frac{1}{2}\lim_{t\to\infty}\frac{\partial\sigma_y^2}{\partial t} = \frac{1}{2}\lim_{t\to\infty}\frac{\partial(\langle y^2\rangle - \langle y\rangle^2)}{\partial t} \\
=& \frac{1}{2}\left\{\frac{1}{2\pi^2}\iint dkdp \begin{pmatrix} 0 \\ (1-f)^2\sin 2k \\ (1-f)^2\cos 2k + f^2 \end{pmatrix}^T (I-\mathcal{M}_{k,p})^{-1}\begin{pmatrix}0\\0\\1\end{pmatrix} + 1\right\} \\
=& \frac{1-f}{2f}\left[\frac{1}{2\pi^2}\iint dkdpR_y(f,k,p) + \frac{f}{1-f}\right] = \frac{1-f}{2f}B_y(f).
\end{aligned}
\tag{36}
$$

The expressions of R_x and R_y can be obtained analytically. Due to the lengthy expressions, we do not present the explicit forms for them here; the detailed expressions for R_x and R_y can be found in Appendix A. The changes in diffusion coefficients D_x and D_y with the coefficient f (dashed red lines) are shown in Figs. 2(a) and 2(b). In addition, the terms B_x and B_y are represented by solid blue lines. We find that when there is no decoherence in the AQW, that is, $f = 0$, both diffusion coefficients, D_x and D_y, are ∞. The motions along the x and y directions exhibit quantum behaviors. With the increase in the coefficient f, the variances along the x direction and y direction both change to increase linearly with time, which means that when the connection has a certain probability of being broken between the adjacent positions of AQW, motions along both the x direction and the y direction exhibit classical behaviors. When the coefficient f approaches 1, the diffusion coefficient along the x direction D_x approaches 0, but the diffusion coefficient along the y direction D_y approaches ∞. That is, when the coefficient f becomes large enough, the only remaining evolution [(IV) in Fig. 1] traps the walker along the x direction with a higher probability, and the other three possible evolutions [(I)–(III) in Fig. 1] are suppressed. At this time, the motion along the x direction has little effect on the motion along the y direction. So as shown in Figs. 2(a) and 2(b), the diffusion coefficient of position in the x direction D_x is close to 0, while in the y direction the diffusion coefficient D_y goes back to ∞ and the motion of the y direction exhibits quantum behavior.

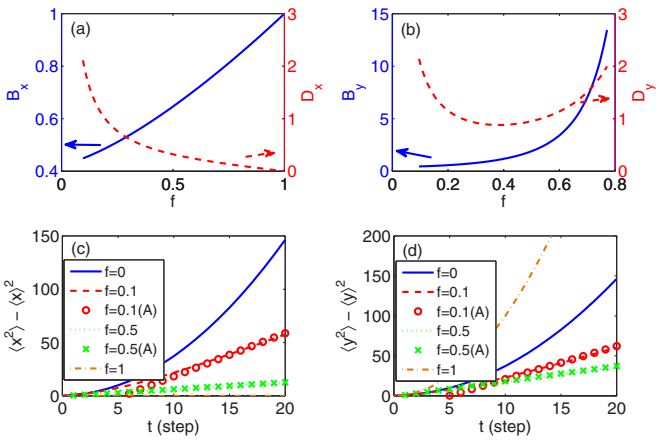

FIG. 2. Diffusion coefficients and variances for a 2D AQW with broken line noise; the noise is applied only along the x direction. (a, b) Diffusion coefficients D_x and D_y with the coefficient f. (c, d) Variances of the position distribution of an AQW with time (step): four f values are presented. Solid line, $f = 0$; dashed red line and open red circle, $f = 0.1$; dotted green line and green cross, $f = 0.5$; dotted-dashed brown line, $f = 1$. Numerical results are represented by solid, dashed, dotted, and dotted-dashed lines. Analytic results from Eqs. (34) and (35) are shown in the forms of red circles and green crosses. In the numerical simulation, the initial state for the 2D walker and coin is $|0\rangle_x|0\rangle_y \otimes (1/\sqrt{2}|R\rangle + i/\sqrt{2}|L\rangle)$.

In Figs. 2(c) and 2(d), we numerically calculate the variances of the position distribution along the x and y directions with time and compare them with the obtained analytic expressions for the variances in the long-time limit [Eqs. (34), (35), and (36)]. In these two figures, four f values are chosen for comparison. The solid blue, dashed red, dotted green, and dotted-dashed brown lines correspond to the variances obtained numerically with coefficient f chosen as 0, 0.1, 0.5, and 1, respectively. The analytic results from Eqs. (34) and (35) are represented by the red circles and green crosses in Figs. 2(c) and 2(d). Our analytic results obtained in Eqs. (34) and (35) coincide with the numerical results when the time becomes longer. In our numerical simulation, we take the initial coin state as $|\psi_0\rangle = 1/\sqrt{2}|R\rangle + i/\sqrt{2}|L\rangle$. From the figures, we find that, when coefficient f is 0 (solid blue lines), motions along both the x direction and the y direction display quantum properties. As coefficient f becomes larger

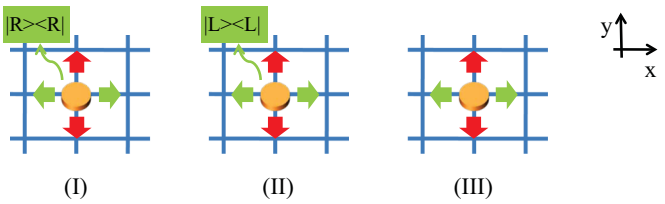

FIG. 3. Schematic of a 2D AQW with coin decoherence; the noise is applied before each step of the walk. Three possible cases of AQW are shown: (I, II) the coin is measured before each step evolution, with probability f; and (III) there is no decoherence in the walk, with probability $1-f$.

(red and green lines), both variances of motion, $\langle x^2\rangle - \langle x\rangle^2$ and $\langle y^2\rangle - \langle y\rangle^2$, change to increase linearly with time, and classical behaviors emerge in both the x and the y directions of the AQW. However, when coefficient f is 1 (brown lines), the spread of the probability distribution along the x direction is trapped at current positions. The variance of motion along the x direction is 0, but the behavior of motion in the y direction returns to showing quantum properties. In Appendix B, we present the expressions of the fitting curves for the numerical values $\langle x^2\rangle - \langle x\rangle^2$ and $\langle y^2\rangle - \langle y\rangle^2$ in Figs. 2(c) and 2(d). For different broken probabilities, the time change of variances in the x direction and y direction in Figs. 2(c) and 2(d) reflect the transitions of motion from quantum to classical behaviors, which are presented in Figs. 2(a) and 2(b).

B. The coin decoherence model

In this section, we study a 2D decoherent AQW where decoherence appears only in the coin space of the walk. Before each step evolution of the 2D AQW, the coin is measured with a certain probability, which makes the coin state decoherence. In our discussion, we assume that coin decoherence emerges with probability f before each step of the walk, then the walker moves along the x direction and y direction in sequence [20]. A schematic of possible evolutions of the AQW involving coin decoherence is depicted in Fig. 3.

In Fig. 3, the walker moving in the x direction (y direction) is labeled by the green arrows along the horizontal direction (red arrows along the vertical direction). The coin decoherence appears before each step of the walk and causes the evolution of a 2D AQW to start with the coin state $|R\rangle$ or $|L\rangle$ [see Fig. 3, (I) and (II), respectively]. The probability of the emergence of such coin decoherence is f. The 2D AQW without decoherence is addressed in Fig. 3, (III), with probability $1-f$. Considering this kind of decoherence, three possible evolutions are associated with three Kraus operators, E_n ($n = 1,2,3$). The explicit expressions of E_n ($n = 1,2,3$) are

$$\begin{aligned} E_1 =& \sqrt{f}\sum_{x,y}\frac{1}{2}\{|x+1,y+1\rangle\langle x,y|\otimes|R\rangle\langle R| + |x+1,y-1\rangle\langle x,y|\otimes|L\rangle\langle R| \\ &+ |x-1,y+1\rangle\langle x,y|\otimes|R\rangle\langle R| - |x-1,y-1\rangle\langle x,y|\otimes|L\rangle\langle R|\}, \end{aligned} \tag{37a}$$

$$\begin{aligned} E_2 =& \sqrt{f}\sum_{x,y}\frac{1}{2}\{|x+1,y+1\rangle\langle x,y|\otimes|R\rangle\langle L| + |x+1,y-1\rangle\langle x,y|\otimes|L\rangle\langle L| \\ &- |x-1,y+1\rangle\langle x,y|\otimes|R\rangle\langle L| + |x-1,y-1\rangle\langle x,y|\otimes|L\rangle\langle L|\}, \end{aligned} \tag{37b}$$

$$\begin{aligned} E_3 =& \sqrt{1-f}\sum_{x,y}\frac{1}{2}\{|x+1,y+1\rangle\langle x,y|\otimes(|R\rangle\langle R| + |R\rangle\langle L|) + |x+1,y-1\rangle\langle x,y|\otimes(|L\rangle\langle R| + |L\rangle\langle L|) \\ &+ |x-1,y+1\rangle\langle x,y|\otimes(|R\rangle\langle R| - |R\rangle\langle L|) - |x-1,y-1\rangle\langle x,y|\otimes(|L\rangle\langle R| - |L\rangle\langle L|\}. \end{aligned} \tag{37c}$$

The operators F_n ($n = 1,2,3$) related to the Kraus operators E_n ($n = 1,2,3$) for the 2D AQW involving coin decoherence can be represented as

$$F_1 = \sqrt{f}\begin{pmatrix} \frac{1}{2}e^{-i(k+p)} + \frac{1}{2}e^{i(k-p)} & 0 \\ \frac{1}{2}e^{-i(k-p)} - \frac{1}{2}e^{i(k+p)} & 0 \end{pmatrix}, \tag{38a}$$

$$F_2 = \sqrt{f}\begin{pmatrix} 0 & \frac{1}{2}e^{-i(k+p)} - \frac{1}{2}e^{i(k-p)} \\ 0 & \frac{1}{2}e^{-i(k-p)} + \frac{1}{2}e^{i(k+p)} \end{pmatrix}, \tag{38b}$$

$$F_3 = \sqrt{1-f}\begin{pmatrix} \frac{1}{2}e^{-i(k+p)} + \frac{1}{2}e^{i(k-p)} & \frac{1}{2}e^{-i(k+p)} - \frac{1}{2}e^{i(k-p)} \\ \frac{1}{2}e^{-i(k-p)} - \frac{1}{2}e^{i(k+p)} & \frac{1}{2}e^{-i(k-p)} + \frac{1}{2}e^{i(k+p)} \end{pmatrix}. \tag{38c}$$

The complete relation is satisfied by $\sum_n F_n^\dagger F_n = I$. Using a technique similar to that mentioned in the section on the broken-line-noise model (Sec. III A), we take a 4×1 column vector to represent the 2×2 matrix, and the expressions for the

superoperators $\mathcal{L}_{k,p}$, $\mathcal{K}_{k,p}$, $\mathcal{P}_{k,p}$, $\mathcal{T}_k$, and $\mathcal{T}_p$ are

$$\mathcal{L}_{k,p}\tilde{O} = \begin{pmatrix} 1 & 0 & 0 & 0 \\ 0 & (1-f)\cos 2p & -(1-f)\cos 2k \sin 2p & \sin 2k \sin 2p \\ 0 & (1-f)\sin 2p & (1-f)\cos 2k \cos 2p & -\sin 2k \cos 2p \\ 0 & 0 & (1-f)\sin 2k & \cos 2k \end{pmatrix} \begin{pmatrix} r_0 \\ r_1 \\ r_2 \\ r_3 \end{pmatrix}, \tag{39}$$

$$\mathcal{K}_{k,p}\tilde{O} = \begin{pmatrix} 0 & i(f-1) & 0 & 0 \\ -i\cos 2p & 0 & (1-f)\sin 2k \sin 2p & \cos 2k \sin 2p \\ -i\sin 2p & 0 & -(1-f)\sin 2k \cos 2p & -\cos 2k \cos 2p \\ 0 & 0 & (1-f)\cos 2k & -\sin 2k \end{pmatrix} \begin{pmatrix} r_0 \\ r_1 \\ r_2 \\ r_3 \end{pmatrix}, \tag{40}$$

$$\mathcal{P}_{k,p}\tilde{O} = \begin{pmatrix} 0 & 0 & i(f-1)\sin 2k & -i\cos 2k \\ 0 & -(1-f)\sin 2p & -(1-f)\cos 2k \cos 2p & \sin 2k \cos 2p \\ 0 & (1-f)\cos 2p & -(1-f)\cos 2k \sin 2p & \sin 2k \sin 2p \\ -i & 0 & 0 & 0 \end{pmatrix} \begin{pmatrix} r_0 \\ r_1 \\ r_2 \\ r_3 \end{pmatrix}, \tag{41}$$

$$\mathcal{T}_k\tilde{O} = \begin{pmatrix} 1 & 0 & 0 & 0 \\ 0 & (1-f)\cos 2p & (1-f)\cos 2k \sin 2p & -\sin 2k \sin 2p \\ 0 & (1-f)\sin 2p & -(1-f)\cos 2k \cos 2p & \sin 2k \cos 2p \\ 0 & 0 & -(1-f)\sin 2k & -\cos 2k \end{pmatrix} \begin{pmatrix} r_0 \\ r_1 \\ r_2 \\ r_3 \end{pmatrix}, \tag{42}$$

$$\mathcal{T}_p\tilde{O} = \begin{pmatrix} 1 & 0 & 0 & 0 \\ 0 & -(1-f)\cos 2p & (1-f)\cos 2k \sin 2p & -\sin 2k \sin 2p \\ 0 & -(1-f)\sin 2p & -(1-f)\cos 2k \cos 2p & \sin 2k \cos 2p \\ 0 & 0 & (1-f)\sin 2k & \cos 2k \end{pmatrix} \begin{pmatrix} r_0 \\ r_1 \\ r_2 \\ r_3 \end{pmatrix}, \tag{43}$$

where $\mathcal{K}_{k,p}^{\dagger}\tilde{O} = \mathcal{K}^{*}\tilde{O}$, $\mathcal{P}_{k,p}^{\dagger}\tilde{O} = \mathcal{P}^{*}\tilde{O}$. With these superoperators, the first moments of position distributions $\langle x\rangle$ and $\langle y\rangle$ in a 2D AQW with coin decoherence are obtained as

$$\begin{aligned} \langle x\rangle &= \frac{i}{2\pi^2}\iint dkdp(-i)(1-f,0,0)\left[\sum_{m=1}^{t}\mathcal{M}_{k,p}^{m-1}\right]\begin{pmatrix} r_1 \\ r_2 \\ r_3 \end{pmatrix} = \frac{1}{2\pi^2}\iint dkdp(1-f,0,0)(I-\mathcal{M}_{k,p})^{-1}\begin{pmatrix} r_1 \\ r_2 \\ r_3 \end{pmatrix}, \\ \langle y\rangle &= \frac{i}{2\pi^2}\iint dkdp(-i)(0,(1-f)\sin 2k,\cos 2k)\left[\sum_{n=1}^{t}\mathcal{M}_{k,p}^{n-1}\right]\begin{pmatrix} r_1 \\ r_2 \\ r_3 \end{pmatrix} \\ &= \frac{1}{2\pi^2}\iint dkdp(0,(1-f)\sin 2k,\cos 2k)(I-\mathcal{M}_{k,p})^{-1}\begin{pmatrix} r_1 \\ r_2 \\ r_3 \end{pmatrix}. \end{aligned} \tag{44}$$

The second moments of position distribution $\langle x^2\rangle$ and $\langle y^2\rangle$ in a 2D AQW with coin decoherence are

$$\begin{aligned} \langle x^2\rangle &= \frac{1}{2\pi^2}\iint dkdp\begin{pmatrix} 1-f \\ 0 \\ 0 \end{pmatrix}^{T}(I-\mathcal{M}_{k,p})^{-1}\{t-\frac{\mathcal{M}_{k,p}}{I-\mathcal{M}_{k,p}}\}\begin{pmatrix} \cos 2p \\ \sin 2p \\ 0 \end{pmatrix} + \frac{1}{2\pi^2}\iint dkdp\frac{1}{2}\cdot t, \\ \langle y^2\rangle &= \frac{1}{2\pi^2}\iint dkdp\begin{pmatrix} 0 \\ (1-f)\sin 2k \\ \cos 2k \end{pmatrix}^{T}(I-\mathcal{M}_{k,p})^{-1}\{t-\frac{\mathcal{M}_{k,p}}{I-\mathcal{M}_{k,p}}\}\begin{pmatrix} 0 \\ 0 \\ 1 \end{pmatrix} + \frac{1}{2\pi^2}\iint dkdp\frac{1}{2}\cdot t. \end{aligned} \tag{45}$$

The diffusion coefficients D_x and D_y are calculated as

$$\begin{aligned} D_x &= \frac{1}{2}\lim_{t\to\infty}\frac{\partial\sigma_x^2}{\partial t} = \frac{1}{2}\lim_{t\to\infty}\frac{\partial(\langle x^2\rangle-\langle x\rangle^2)}{\partial t} = \frac{1}{2}\left\{\frac{1}{2\pi^2}\iint dkdp\begin{pmatrix} 1-f \\ 0 \\ 0 \end{pmatrix}^{T}(I-\mathcal{M}_{k,p})^{-1}\begin{pmatrix} \cos 2p \\ \sin 2p \\ 0 \end{pmatrix} + \frac{1}{2\pi^2}\iint dkdp\frac{1}{2}\right\} \\ &= \frac{1-f}{2f}\left[\frac{1}{2\pi^2}\iint dkdpR_x(f,k,p) + \frac{f}{1-f}\right] = \frac{1-f}{2f}B_x(f), \\ D_y &= \frac{1}{2}\lim_{t\to\infty}\frac{\partial\sigma_y^2}{\partial t} = \frac{1}{2}\lim_{t\to\infty}\frac{\partial(\langle y^2\rangle-\langle y\rangle^2)}{\partial t} = \frac{1}{2}\left\{\frac{1}{2\pi^2}\iint dkdp\begin{pmatrix} 0 \\ (1-f)\sin 2k \\ \cos 2k \end{pmatrix}^{T}(I-\mathcal{M}_{k,p})^{-1}\begin{pmatrix} 0 \\ 0 \\ 1 \end{pmatrix} + \frac{1}{2\pi^2}\iint dkdp\frac{1}{2}\right\} \\ &= \frac{1-f}{2f}\left[\frac{1}{2\pi^2}\iint dkdpR_y(f,k,p) + \frac{f}{1-f}\right] = \frac{1-f}{2f}B_y(f). \end{aligned} \tag{46}$$

Here, the term $R_x = \frac{1-f+\cos 2p}{2-f}$, and $R_y = \frac{-2(1-f)\cos 2p \cot^2 k+[(1-f)^2+\cos 2k]\csc^2 k}{2(2-3f+f^2)}$.

We find that the function $R_y(f,k,p)$ approaches ∞ at some values of k and p for any value of f, which makes the amplitude of the diffusion coefficients D_y approach ∞. This means that the motion along the y direction always exhibits quantum behavior, whatever probability f is taken. The diffusion coefficient D_x with a change in the probability f is presented in Fig. 4(a). The diffusion coefficient D_x is represented by the dashed red line, and the term B_x by the solid blue line. For a walker traveling along the x direction, with an increase in the probability f, the effect of decoherence on the system becomes stronger, and the variance along the x direction reveals the linear time dependence on time t. When the probability f approaches 1, the motion along the x direction exhibits classical behavior with the diffusion coefficient D_x equal to 1/2. The variances of the position distribution along the x and y directions reveal different dependences on the decoherent strength f. In our study, coin decoherence appears before each step of the walk, the coherence of the coin is lost, and the motion along the x direction is affected, but the motion along the y direction feels little effect and always displays quantum behavior with a change in the probability f. In Figs. 4(b) and 4(c), we numerically calculate the variance of the position distribution along the x and y directions of the 2D AQW involving coin decoherence with time. The obtained analytic expressions for the variance in the long-time limit [Eqs. (44)–(46)] are presented for comparison. Four probabilities f are chosen. The solid blue, dashed red, dotted green, and dotted-dashed brown lines correspond to probabilities $f = 0$, $f = 0.1$, $f = 0.5$, and $f = 1$, respectively. In these two figures, with an increase in the probability f, the decoherence becomes stronger ($f = 0.5$ and $f = 1$); we find that the variance along the x direction changes to increase linearly with time. Motion in this direction displays classical behaviors. The analytic results from Eqs. (44) and (45) are represented by green circles and brown crosses in Fig. 4(b). In comparison, motion along the y direction always exhibits quantum behaviors for any value of probability f [see Fig. 4(c)]. Our numerical results in Figs. 4(b) and 4(c) coincide with the statements in Fig. 4(a). In Appendix B, we present the expressions of the fitting curves for the numerical values $\langle x^2\rangle - \langle x\rangle^2$ and $\langle y^2\rangle - \langle y\rangle^2$ in Figs. 4(b) and 4(c). Comparing the 2D AQW involving broken line noise and coin decoherence, different behaviors for variances of position distributions have been uncovered. In the former case, the decoherence affects both the coin and the position; when decoherence in the x direction occurs, motion along the x direction has an influence on the state of the coin, which in turn affects the motion along the y direction. However, in the latter case, the decoherence affects only the coin before each step of the walk; motion along the y direction is influenced little by the coin decoherence in the 2D AQW. So motion along the y direction maintains its quantum properties with a change in decoherence strength f.

To illustrate the effects of different kinds of decoherence and reveal the anisotropic behaviors in the position space, we present the probability distributions in the x-y position space of a 2D AQW with different f values in Fig. 5.

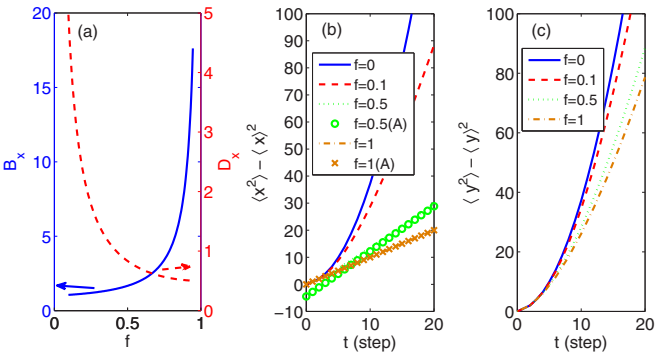

FIG. 4. Diffusion coefficients and variances for a 2D AQW with coin decoherence; noise is applied before each step of the walk. (a) Diffusion coefficient D_x (dashed red line) and B_x (solid blue line) with probability f. (b, c) Variances of the position distribution of the AQW with time (step). Four probabilities f are shown: solid blue line, $f = 0$; dashed red line, $f = 0.1$; dotted green line, $f = 0.5$; and dotted-dashed brown line, $f = 1$. Analytic results for the variance in the long-time limit are represented by green circles and brown crosses in (b). The initial state for the 2D walker and coin is $|0\rangle_x|0\rangle_y \otimes (1/\sqrt{2}|R\rangle + i/\sqrt{2}|L\rangle)$.

Figures 5(a)– 5(c) describe the position distribution of the 2D AQW with broken line noise, and Figs. 5(d)– 5(f) denote the case of the 2D decoherent AQW with coin decoherence. The time steps in all panels are 20. As one coin has been tossed twice in one step evolution of the 2D AQW, these position distributions are different from those of the four-level coin decoherent Grover walk [26]. In our study, three probabilities f are chosen: $f = 0$, Figs. 5(a) and 5(d); $f = 0.5$, Figs. 5(b) and 5(e); and $f = 1$, Figs. 5(c) and 5(f). Compared with the 2D AQW without decoherence [$f = 0$; Figs. 5(a) and 5(d)], when decoherence is introduced [Figs. 5(b), 5(c), 5(e), and 5(f)], the interference pattern of the probability distribution in the AQW changes, and the anisotropic distribution in the x-y position space of 2D AQW can be found. With an increase in the probability f [Figs. 5(b) and 5(e)], the position distribution does not show the complex, oscillatory form as described for

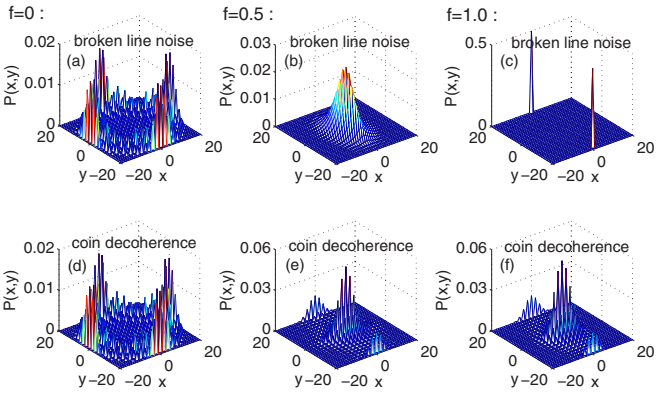

FIG. 5. Probability distribution in the position space x-y of a 2D AQW involving two kinds of decoherence at time step $t = 20$. (a–c) Broken line noise is introduced in the x direction; (d–f) coin decoherence is applied to the coin before each step of the walk. Three probabilities f are shown: (a, d) $f = 0$; (b, e), $f = 0.5$; and (c, f) $f = 1$. The initial state for the 2D walker and the coin is $|0\rangle_x|0\rangle_y \otimes (1/\sqrt{2}|R\rangle + i/\sqrt{2}|L\rangle)$.

the coherent QW. When the probability f is 1, because the walk is affected by broken line noise [Fig. 5(c)], the Kraus operators $\{E_n,\ n = 1,2,3,4\}$ of one step evolution of the 2D AQW change to $E_4 = \sum_{x,y}(|y+1,x\rangle\langle y,x| \otimes |R\rangle\langle R| - |y-1,x\rangle\langle y,x| \otimes |L\rangle\langle L|$ only; the calculation details are presented in Appendix C. In this case, the position distribution along the x direction is trapped, which coincides with 0 for the variance of position distribution along the x direction (Fig. 2). The position distribution along the y direction still spreads with time. For the walk with coin decoherence [Fig. 5(f)], it is clearly seen that the position distribution along the y direction spreads more rapidly than that along the x direction. When $f = 1$, that means the coin is measured definitely before each step of the walk, and the Kraus operators $\{E_n,\ n = 1,2,3\}$ for the 2D AQW with coin decoherence decrease to E_1 and E_2. (The detailed expressions of E_1 and E_2 are given in Appendix C.) In this case, the pattern along the x direction reveals the classical binomial distribution [Fig. 4(b)]. Though some of the probability along the y direction of the walk appears around the origin point, the motion along the y direction reveals some quantum behaviors [Fig. 4(c)].

IV. CORRELATIONS OF THE TWO-DIMENSIONAL AQW IN THE PRESENCE OF DECOHERENCE

When taking decoherence into account, we have discussed the anisotropic position distribution in the 2D AQW. In this section, we quantitatively estimate the correlation between the 2D walker and the coin in the presence of decoherence. Exploiting the correlations reserved in the AQW is a very interesting problem; it will uncover how many correlations survive when decoherence is introduced and might have applications in the process of quantum information. The entanglement between two one-dimensional quantum walkers has been studied in Ref. [5], and the effects of initial entangled coin states have been analyzed in Refs. [47] and [48]. In this section, first, we study the time evolution of correlations between the x direction and the y direction (two orthogonal directions) of a 2D AQW in which the walker is moving. The classical mutual information is chosen to measure the classical correlation, and we use the measurement-induced disturbance (MID) to qualify the quantum correlation [49–51]. Second, we qualify the quantum correlations stored between the position of the 2D walker and the state of the coin. The definition of the classical mutual information $I_c(t)$ is presented below to measure the information shared by the x and y directions of the 2D AQW in which the 2D walker is moving:

$$I_c(t) = \sum_x \sum_y P(x,y,t) \log_2 \left(\frac{P(x,y,t)}{P(x,t)P(y,t)} \right). \tag{47}$$

Here, $P(x,y,t)$ denotes the probability of the 2D walker's occupying position (x,y) in the x-y position space at time t. The marginal probability distribution $P(x,t)$ stands for the probability of the 2D walker's occupying position x at time t, and the marginal probability distribution $P(y,t)$ represents the probability of the 2D walker's occupying position y at time t. When the correlation between the x and the y position of 2D AQW is 0, the shared information I_c is 0.

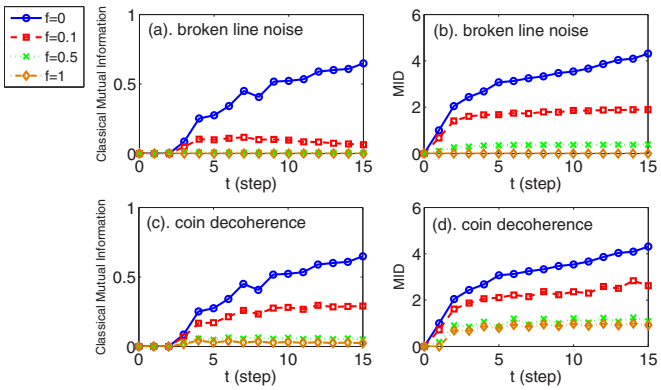

FIG. 6. Classical and quantum correlations between the x direction and the y direction of a 2D AQW in which the 2D walker is moving. (a, b) Broken line noise is introduced in the x direction; (c, d) coin decoherence is applied to the coin before each step of the walk. The classical correlation is represented by classical mutual information, shown in (a) and (c). In (b) and (d), lines for the quantum correlation represented by MID are shown. Four probabilities f are shown: blue circles, $f = 0$; red rectangles, $f = 0.1$; green crosses, $f = 0.5$; and brown diamonds, $f = 1$. The initial state for the 2D walker and the coin is $|0\rangle_x|0\rangle_y \otimes (1/\sqrt{2}|R\rangle + i/\sqrt{2}|L\rangle)$.

For the quantum correlation, though it is well estimated by quantum discord, it might be difficult to evaluate because of the requirement of minimization over possible measurements [49,50]. Here, we use the MID $Q(\rho)$ to estimate the quantum correlation [50]; that is,

$$Q(\rho) = I(\rho) - I(\Pi\rho), \tag{48}$$

with

$$I(\rho) = S(\rho_1) + S(\rho_2) - S(\rho), \tag{49}$$

where $S(\rho) = -\mathrm{Tr}(\rho \log_2 \rho)$. The state $\Pi\rho$ satisfies $\Pi\rho = \sum_{j,k} \Pi_1^j \otimes \Pi_2^k \rho \Pi_1^j \otimes \Pi_2^k$. The projectors $\{\Pi_1^j\}$ and $\{\Pi_2^k\}$ represent the complete projective measurements which are performed on parties 1 and 2 of bipartite state ρ, respectively. We have the complete relations as $\rho_1 = \sum_j p_1^j \Pi_1^j$ and $\rho_2 = \sum_k p_2^k \Pi_2^k$. The reduced density matrices ρ_1 and ρ_2 are expressed as $\rho_1 = \mathrm{Tr}_2\rho$ and $\rho_2 = \mathrm{Tr}_1\rho$, respectively.

In Fig. 6, we present the time evolutions of classical mutual information and MID between the x and the y positions of the 2D walker. Figures 6(a) and 6(b) represent the 2D AQW affected by broken line noise, and Figs. 6(c) and 6(d) the 2D AQW with coin decoherence. Four probabilities f are chosen for comparison. The 2D AQW without decoherence ($f = 0$) is depicted by blue circles. Lines with red rectangles, green crosses, and brown diamonds correspond to the 2D AQW with probabilities $f = 0.1$, $f = 0.5$, and $f = 1$. When there is no decoherence in the AQW (blue circles in Fig. 6), correlations between the x and the y positions of the 2D walker are strong. Under the influence of noises (red rectangles, green crosses, and brown diamonds in Fig. 6), correlations between the x and the y positions of the 2D walker decrease. For the broken-line-noise model, when the probability f approaches 1 [brown diamonds in Figs. 6(a) and 6(b)], the classical and quantum correlations between the x and the y positions of the 2D walker are close to 0. As shown in Fig. 5(c), the probability distribution

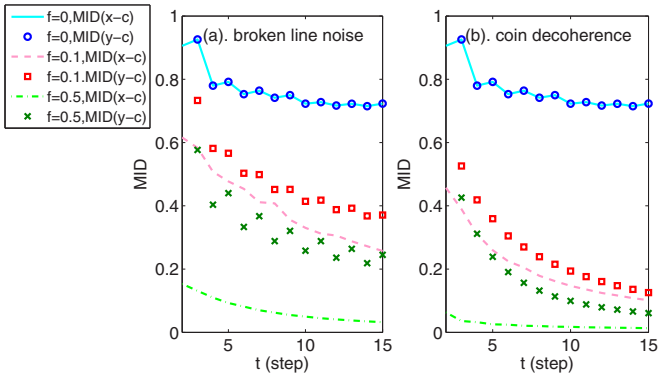

FIG. 7. Quantum correlations between the x (y) position of the 2D walker and the state of the coin in the presence of decoherence. (a) Broken line noise is introduced in the x direction; (b) coin decoherence is applied to the coin before each step of the walk. The quantum correlation is represented by MID. Three probabilities f are shown. For the correlation between the x position of the walker and the coin MID(x-c), light-blue solid line, $f = 0$; light-red dashed line, $f = 0.1$; and light-green dashed-dotted line, $f = 0.5$. For the correlation between the y position of the walker and the coin MID(y-c), dark-blue circles, $f = 0$; dark-red rectangles, $f = 0.1$; and dark-green crosses, $f = 0.5$. The initial state for the 2D walker and the coin is $|0\rangle_x|0\rangle_y \otimes (1/\sqrt{2}|R\rangle + i/\sqrt{2}|L\rangle)$.

of the AQW is trapped along the x direction. This localization of the distribution reduces the correlation between the x and the y positions of the walker to 0 and makes the 2D walker travel along the x direction and y direction independently and share no information. When coin decoherence is introduced in the AQW [Figs. 6(c) and 6(d)], compared to the no-decoherence AQW, the correlation between the x and the y positions of the 2D walker decreases to a smaller value. When the probability f is close to 1 [brown diamonds in Figs. 6(c) and 6(d)], the correlations between the x and the y positions of the 2D walker are not 0. As mentioned above, coin decoherence disturbs the 2D AQW weakly, and the motion in the y direction exhibits quantum behavior whatever value of the probability f is taken. This weak decoherence affects the movement of the 2D walker and keeps some correlations between the x and the y directions of the 2D AQW in which the 2D walker is moving.

Later, we qualify the correlations between the position of the 2D walker and the state of the coin. In our discussion, we study the quantum correlations estimated by MID. The correlation between the x position of the walker and the coin is represented by MID(x-c); the correlation between the y position of the walker and the coin is expressed as MID(y-c) (see Fig. 7).

The time evolutions of quantum correlations MID(x-c) and MID(y-c) are shown in Fig. 7. Three probabilities f are chosen to illustrate the decoherence effect. For MID(x-c), the light-blue solid, light-red dashed, and light-green dotted-dashed lines correspond to probabilities $f = 0$, $f = 0.1$, and $f = 0.5$, respectively. For MID(y-c), the dark-blue circles, dark-red rectangles, and dark-green crosses correspond to probabilities $f = 0$, $f = 0.1$, and $f = 0.5$, respectively. As shown in Figs. 7(a) and 7(b), with an increase in the probability f, both quantum correlations, MID(x-c) and MID(y-c), decrease. Because decoherence appears in only one direction of the 2D AQW, the anisotropic quantum correlations between the x (y) position of the walker and the state of the coin emerge. In Figs. 7(a) and 7(b), we see that, when there is no decoherence [solid blue lines and blue circles in Figs. 7(a) and 7(b)], the quantum correlations MID(x-c) and MID(y-c) have the same amplitudes with time. When broken line noise (coin decoherence) is introduced into the walk, because the decoherence emerges only in the x direction (decoherence appears only before each step of the walk), the quantum correlation between the x position of the walker and the state of the coin MID(x-c) is affected more strongly than that between the y position of the walker and the state of the coin MID(y-c). The remaining quantum correlation MID(y-c) is larger than the correlation MID(x-c). Considering the variances of position distribution discussed above, when two kinds of decoherence (broken line noise and coin decoherence) are introduced, the behavior along the y direction of the 2D AQW exhibits more "quantumness" than that along the x direction of the 2D AQW. Such anisotropic quantum correlations, MID(x-c) and MID(y-c), correspond to the aforementioned anisotropic position distribution patterns of the 2D AQW.

V. CONCLUSIONS

In this paper, we have studied the dynamics of the 2D alternative quantum walk (AQW) in the presence of decoherence. We present the analytic expressions for the first and second moments of the position distribution involving different kinds of decoherence. The emergence of quantum and classical behaviors in the AQW are discussed. Taking broken line noise and coin decoherence as examples of decoherence, we analyze the diffusion coefficients and the variances of position distribution in the 2D AQW. We find that, when broken line noise is applied to the system, the motions along the x and y directions both change to exhibit classical behaviors. When the broken probability f approaches 1, movement in the x direction is trapped, and motion along the y direction displays quantum behaviors. In comparison, when coin decoherence is introduced into the walk, the coin is influenced by this weak decoherence, and only the dynamics along one direction is affected. In our study, we find that classical behaviors emerge in motion along the x direction, but motion along the y direction exhibits quantum behaviors, whatever the strength of decoherence taken.

In addition, we discuss the correlations between the x (y) position of the 2D walker and the state of the coin in the 2D AQW. First, we employ the classical mutual information and measurement-induced disturbance (MID) to qualify the classical and quantum correlations between the x and the y positions of the 2D walker. We find that, with the appearance of decoherence, the correlations between the x and the y positions of the walker are smaller than those with no decoherence. For the broken-line-noise model, when the broken probability is close to 1, the trap of the position distribution causes no correlations to exist. However, for the case of coin decoherence, such decoherence weakly disturbs the coherent evolution of the system, and the correlations between the x and the y positions of the walker still exist no matter how strong the decoherence is. Second, we discuss the quantum correlation between the x (y) position of the walker

and the state of the coin. When decoherence is introduced into the walk, the anisotropic quantum correlations between the x (y) position of the walker and the state of the coin emerge, which correspond to the anisotropic position distribution of the 2D AQW in the presence of decoherence.

Due to the reduced resources required for experimental realization, the 2D AQW has its advantage in designing quantum search algorithms. For real experimental realizations, the decoherence effect from the surrounding environment is unavoidable. In this paper, we study the 2D AQW involving decoherence in detail. Our results provide the theoretical basis for the development of quantum algorithms based on the 2D AQW in real experimental realizations.

ACKNOWLEDGMENTS

We acknowledge financial support from Young Teachers Academic Starting Plan No. 2015CX04046 of Beijing Institute of Technology.

APPENDIX A: THE EXPRESSIONS OF R_x AND R_y

For a 2D AQW with broken line noise, we have provided the diffusion coefficients D_x and D_y in Eq. (36). The detailed expressions $R_x(f,k,p)$ and $R_y(f,k,p)$ are

$$R_x(f,k,p) = \frac{1+f(-3+4f)+2(-1+f)\cos 2k\cos^2 p+(1+f)\cos 2p+2f\sin k\sin 2p}{3+f(-5+4f)+2(-1+f)\cos 2k\cos^2 p+(-1+3f)\cos 2p+2(-1+f)\sin k\sin 2p} \tag{A1}$$

and

$$R_y(f,k,p) = \frac{A_1 + A_2 * A_3}{A_4}, \tag{A2}$$

where the explicit forms of A_1, A_2, A_3, and A_4 are

$$\begin{aligned}
A_1 &= 2*(1-f)^2\cos k\sin 2k[(1-f)(1-2f-\cos 2p)\sin k + f\sin 2p],\\
A_2 &= \frac{f^2+(1-f)^2\cos 2k}{f-1},\\
A_3 &= -1+f^2-2f^3+(1-2f-f^2)\cos 2p-(1-f)^2\cos 2k(1-2f-\cos 2p)+2(1-f)f\sin k\sin 2p,\\
A_4 &= 2*(1-f)[3+f(4f-5)+2(f-1)\cos 2k\cos^2 p+(3f-1)\cos 2p+2(f-1)\sin k\sin 2p].
\end{aligned} \tag{A3}$$

APPENDIX B: THE EXPRESSIONS OF FITTING CURVES FOR THE VARIANCES $\langle x^2\rangle - \langle x\rangle^2$ AND $\langle y^2\rangle - \langle y\rangle^2$

In this Appendix, we present the expressions of fitting curves for the numerically obtained variances $\langle x^2\rangle - \langle x\rangle^2$ and $\langle y^2\rangle - \langle y\rangle^2$ [Figs. 2(c) and 2(d) and Figs. 4(b) and 4(c), respectively.). The time interval for the fitting curves is chosen between 0 and 20. For the variances of a 2D AQW with broken line noise [Figs. 2(c) and 2(d)], the expressions of the fitting curves are listed in Table I. We also list the coefficients for different orders of time t in fitting curves in the table.

Then we discuss the variances of a 2D AQW with coin decoherence and present the expressions of fitting curves for the obtained numerical values of variances [Figs. 4(b) and 4(c)]. The coefficients for different orders of time t in fitting curves are listedin Table II.

The coefficients of determination R^2 for all of the fitting curves are larger than 0.999. From the coefficients presented above, we find that in some cases, the variances change to increase linearly with time when decoherence is considered, while when coin decoherence is introduced before each step of the walk, the variance $\langle y^2\rangle - \langle y\rangle^2$ always maintains its quadratic dependence on time t [Fig. 4(c)].

TABLE I. The broken-line-noise model: Coefficients for different orders of time t.

	t^2	t^1	t^0
$\langle x^2\rangle - \langle x\rangle^2$, $f=0$	0.360	0.080	0.364
$\langle x^2\rangle - \langle x\rangle^2$, $f=0.1$	0.071	1.578	−1.405
$\langle x^2\rangle - \langle x\rangle^2$, $f=0.5$	0.001	0.595	−0.138
$\langle x^2\rangle - \langle x\rangle^2$, $f=1$	0	0	0
$\langle y^2\rangle - \langle y\rangle^2$, $f=0$	0.360	0.080	0.364
$\langle y^2\rangle - \langle y\rangle^2$, $f=0.1$	0.071	1.715	−1.463
$\langle y^2\rangle - \langle y\rangle^2$, $f=0.5$	0.007	1.713	−0.713
$\langle y^2\rangle - \langle y\rangle^2$, $f=1$	1.000	0	0

TABLE II. The coin decoherence model: Coefficients for different orders of time t

	t^2	t^1	t^0
$\langle x^2\rangle - \langle x\rangle^2$, $f=0$	0.360	0.080	0.364
$\langle x^2\rangle - \langle x\rangle^2$, $f=0.1$	0.155	1.454	−1.402
$\langle x^2\rangle - \langle x\rangle^2$, $f=0.5$	0.010	1.308	−0.496
$\langle x^2\rangle - \langle x\rangle^2$, $f=1$	0	1.000	0
$\langle y^2\rangle - \langle y\rangle^2$, $f=0$	0.360	0.080	0.364
$\langle y^2\rangle - \langle y\rangle^2$, $f=0.1$	0.279	0.707	−0.486
$\langle y^2\rangle - \langle y\rangle^2$, $f=0.5$	0.159	1.333	−1.052
$\langle y^2\rangle - \langle y\rangle^2$, $f=1$	0.131	1.391	−1.006

APPENDIX C: THE EMERGENCE OF QUANTUM BEHAVIORS AT $f = 1$

We discuss the emergence of quantum behaviors at $f = 1$ in this Appendix. For a 2D AQW with broken line noise, we find that motion along y direction exhibits quantum properties when $f = 1$ [see Figs. 2(d) and 5(c)]. In this case, the conditional shift operator along the x direction is

$$S^4_{x,b} = \sum_x |x\rangle\langle x| \otimes (|R\rangle\langle L| + |L\rangle\langle R|), \tag{C1}$$

and the Kraus operators $\{E_n,\ n = 1,2,3,4\}$ change to E_4 only:

$$E_4 = S_y(I \otimes H)S^4_{x,b}(I \otimes H) = \sum_{x,y}(|x,y+1\rangle\langle x,y| \otimes |R\rangle\langle R| - |x,y-1\rangle\langle x,y| \otimes |L\rangle\langle L|). \tag{C2}$$

After applying the Kraus operator E_4 to this initial state, motion along the x direction is trapped and motion along the position or negative y direction is determined by the coin state $|R\rangle$ or $|L\rangle$. In the text, the initial state for the 2D AQW is $|0\rangle_x|0\rangle_y \otimes (1/\sqrt{2}|R\rangle + i/\sqrt{2}|L\rangle)$, and the position distribution along the y direction is peaked at the edges of the y-coordinate axis, which is presented in Fig. 5(c).

For a 2D AQW with coin decoherence, the probability $f = 1$ means that the coin is measured definitely before each step of the walk, and the evolution of the 2D AQW starts with the coin state $|R\rangle$ or $|L\rangle$. In Fig. 4, we find that motion along the y direction reveals quantum properties. When $f = 1$, the Kraus operators $\{E_n,\ n = 1,2,3\}$ change to E_1 and E_2:

$$\begin{aligned}
E_1 &= S_y(I \otimes H)S_x(I \otimes H)|R\rangle\langle R| \\
&= \frac{1}{2}\sum_{x,y}[|x+1,y+1\rangle\langle x,y| \otimes |R\rangle\langle R| + |x+1,y-1\rangle\langle x,y| \otimes |L\rangle\langle R| \\
&\quad +|x-1,y+1\rangle\langle x,y| \otimes |R\rangle\langle R| - |x-1,y-1\rangle\langle x,y| \otimes |L\rangle\langle R|], \\
E_2 &= S_y(I \otimes H)S_x(I \otimes H)|L\rangle\langle L| \\
&= \frac{1}{2}\sum_{x,y}[|x+1,y+1\rangle\langle x,y| \otimes |R\rangle\langle L| + |x+1,y-1\rangle\langle x,y| \otimes |L\rangle\langle L| \\
&\quad -|x-1,y+1\rangle\langle x,y| \otimes |R\rangle\langle L| + |x-1,y-1\rangle\langle x,y| \otimes |L\rangle\langle L|].
\end{aligned} \tag{C3}$$

Here, we consider two cases. First, we assume that the conditional shift operator S_x is omitted; the Kraus operators E_1 and E_2 change to

$$\begin{aligned}
E'_1 &= S_y(I \otimes H)(I \otimes H)|R\rangle\langle R| = \sum_y(|y+1\rangle\langle y| \otimes |R\rangle\langle R| + |y-1\rangle\langle y| \otimes |L\rangle\langle L|)|R\rangle\langle R| \\
&= \sum_y |y+1\rangle\langle y| \otimes |R\rangle\langle R|, \\
E'_2 &= S_y(I \otimes H)(I \otimes H)|L\rangle\langle L| = \sum_y(|y+1\rangle\langle y| \otimes |R\rangle\langle R| + |y-1\rangle\langle y| \otimes |L\rangle\langle L|)|L\rangle\langle L| \\
&= \sum_y |y-1\rangle\langle y| \otimes |L\rangle\langle L|.
\end{aligned} \tag{C4}$$

In this case, we find that when the coin state is $|R\rangle$ ($|L\rangle$), the walker travels only along the positive (negative) y direction. Second, we assume that the conditional shift operator S_y and one coin operator H are omitted; the Kraus operators E_1 and E_2 change to

$$\begin{aligned}
E''_1 &= S_x(I \otimes H)|R\rangle\langle R| = \frac{1}{\sqrt{2}}\sum_x(|x+1\rangle\langle x| \otimes |R\rangle\langle R| + |x-1\rangle\langle x| \otimes |L\rangle\langle R|), \\
E''_2 &= S_x(I \otimes H)|L\rangle\langle L| = \frac{1}{\sqrt{2}}\sum_x(|x+1\rangle\langle x| \otimes |R\rangle\langle L| - |x-1\rangle\langle x| \otimes |L\rangle\langle L|).
\end{aligned} \tag{C5}$$

From these two operators, E''_1 and E''_2, no matter what state the coin is, the walker has equal probability of traveling along the positive or negative x direction. The classical probability distribution along the x direction emerges with these two operators, E''_1 and E''_2. For a 2D AQW with coin decoherence, when $f = 1$, two Kraus operators for one step evolution are E_1 and E_2. In the text, the initial state for the 2D AQW is $|\psi_0\rangle = |0\rangle_x|0\rangle_y \otimes (1/\sqrt{2}|R\rangle + i/\sqrt{2}|L\rangle)$. Compared with the operators E''_1 and E''_2, due to the emergence of the same operators, $S_x(I \otimes H)|R\rangle\langle R|$ and $S_x(I \otimes H)|L\rangle\langle L|$, in E_1 and E_2, we find that motion along the x direction exhibits classical behavior in the 2D AQW with coin decoherence [see the case where $f = 1$ in Figs. 4(b) and 5(f)]. Considering the evolution with operators E'_1 and E'_2, when the coin state is $|R\rangle$ or $|L\rangle$, the walker travels only along the

positive or negative y direction. With the initial state of the walk $|\psi_0\rangle$, the probability distribution is peaked at the edges of the y-coordinate axis. In this case, the variance of the position distribution grows quadratically with time, which is not a characteristic of the classical walk. When the conditional shift operator S_x is added into E_1' and E_2', the operators change to E_1 and E_2, and the interaction between the x direction and the y direction is established. Compared with the evolution with operators E_1' and E_2', though some of the probability distribution along the y direction returns to the point of origin with operators E_1 and E_2, motion along the y direction still exhibits quantum behavior [see the case where $f = 1$ in Figs. 4(c) and 5(f)].

[1] J. Kempe, Contemp. Phys. **44**, 307 (2003).
[2] S. E. Venegas-Andraca, Quant. Info. Proc. **11**, 1015 (2012).
[3] E. Farhi and S. Gutmann, Phys. Rev. A **58**, 915 (1998).
[4] Y. Aharonov, L. Davidovich, and N. Zagury, Phys. Rev. A **48**, 1687 (1993).
[5] T. D. Mackay, S. D. Bartlett, L. T. Stephenson, and B. C. Sanders, J. Phys. A **35**, 2745 (2002).
[6] N. Inui, Y. Konishi, and N. Konno, Phys. Rev. A **69**, 052323 (2004).
[7] A. M. Childs, Phys. Rev. Lett. **102**, 180501 (2009).
[8] A. M. Childs, D. Gosset, and Z. Webb, Science **339**, 791 (2013).
[9] A. M. Childs, E. Farhi, and S. Gutmann, Quant. Info. Proc. **1**, 35 (2002).
[10] N. Shenvi, J. Kempe, and K. B. Whaley, Phys. Rev. A **67**, 052307 (2003).
[11] A. M. Childs and J. Goldstone, Phys. Rev. A **70**, 022314 (2004).
[12] A. Ambainis, J. Kempe, and A. Rivosh, *SODA '05: Proceedings of the Sixteenth Annual ACM-SIAM Symposium on Discrete Algorithms* (Society for Industrial and Applied Mathematics, Philadelphia, PA, 2005), p. 1099.
[13] A. Tulsi, Phys. Rev. A **78**, 012310 (2008).
[14] V. Potoček, A. Gábris, T. Kiss, and I. Jex, Phys. Rev. A **79**, 012325 (2009).
[15] G. Abal, R. Donangelo, F. L. Marquezino, and R. Portugal, Math. Struct. Comput. Sci. **20**, 999 (2010).
[16] J. Ghosh, Phys. Rev. A **89**, 022309 (2014).
[17] C. Lyu, L. Yu, and S. Wu, Phys. Rev. A **92**, 052305 (2015).
[18] T. Chen and X. Zhang, Sci. Rep. **6**, 25767 (2016).
[19] T. A. Brun, H. A. Carteret, and A. Ambainis, Phys. Rev. Lett. **91**, 130602 (2003).
[20] T. A. Brun, H. A. Carteret, and A. Ambainis, Phys. Rev. A **67**, 032304 (2003).
[21] D. Shapira, O. Biham, A. J. Bracken, and M. Hackett, Phys. Rev. A **68**, 062315 (2003).
[22] A. Romanelli, R. Siri, G. Abal, A. Auyuanet, and R. Donangelo, Physica A **347**, 137 (2005).
[23] L. Ermann, J. P. Paz, and M. Saraceno, Phys. Rev. A **73**, 012302 (2006).
[24] J. Košík, V. Bužek, and M. Hillery, Phys. Rev. A **74**, 022310 (2006).
[25] N. V. Prokof'ev and P. C. E. Stamp, Phys. Rev. A **74**, 020102(R) (2006).
[26] A. C. Oliveira, R. Portugal, and R. Donangelo, Phys. Rev. A **74**, 012312 (2006).
[27] V. Kendon, Math. Struct. Comput. Sci. **17**, 1169 (2007).
[28] G. Abal, R. Donangelo, F. Severo, and R. Siri, Physica A **387**, 335 (2008).
[29] A. Romanelli, Phys. Rev. A **80**, 042332 (2009).
[30] M. Annabestani, S. J. Akhtarshenas, and M. R. Abolhassani, Phys. Rev. A **81**, 032321 (2010).
[31] C. Liu and N. Petulante, Phys. Rev. E **81**, 031113 (2010).
[32] C. Liu and N. Petulante, Phys. Rev. A **84**, 012317 (2011).
[33] A. Romanelli, and G. Hernández, Physica A **390**, 1209 (2011).
[34] C. Ampadu, Commun. Theor. Phys. **57**, 41 (2012).
[35] P. Xue and B. C. Sanders, Phys. Rev. A **87**, 022334 (2013).
[36] C. Di Franco, M. McGettrick, and Th. Busch, Phys. Rev. Lett. **106**, 080502 (2011).
[37] C. Di Franco, M. McGettrick, T. Machida, and Th. Busch, Phys. Rev. A **84**, 042337 (2011).
[38] E. Roldán, C. Di Franco, F. Silva, and G. J. de Valcárcel, Phys. Rev. A **87**, 022336 (2013).
[39] B. Kollár, T. Kiss, and I. Jex, Phys. Rev. A **91**, 022308 (2015).
[40] C. Di Franco and M. Paternostro, Phys. Rev. A **91**, 012328 (2015).
[41] A. Schreiber *et al.*, Science **336**, 55 (2012).
[42] Y.-C. Jeong, C. Di Franco, H.-T. Lim, M. S. Kim, and Y.-H. Kim, Nat. Commun. **4**, 2471 (2013).
[43] J. Svozilík, R. de J. León-Montiel, and J. P. Torres, Phys. Rev. A **86**, 052327 (2012).
[44] C. M. Chandrashekar, arXiv:1212.5984.
[45] C. M. Chandrashekar and T. Busch, J. Phys. A **46**, 105306 (2013).
[46] M. Nielsen and I. Chuang, *Quantum Computation and Quantum Information* (Cambridge University Press, Cambridge, UK, 2000).
[47] Y. Omar, N. Paunković, L. Sheridan, and S. Bose, Phys. Rev. A **74**, 042304 (2006).
[48] L. Sheridan, N. Paunković, Y. Omar, and S. Bose, Int. J. Quantum. Inform. **4**, 573 (2006).
[49] H. Ollivier and W. H. Zurek, Phys. Rev. Lett. **88**, 017901 (2002).
[50] S. Luo, Phys. Rev. A **77**, 022301 (2008).
[51] P. Xue and B. C. Sanders, Phys. Rev. A **85**, 022307 (2012).